fibers

MDPI

Article

Aging Effects on Flexural Behavior of Glass Fiber-Reinforced Stone-Cork Composite Panels for External Facade Elements

João Marques [1,2,*], Madalena Barata Garcia [3], Virgínia Infante [4], Pedro Miguel Amaral [4] and Arménio Correia [3]

[1] Mechanical Engineering (DEM), Escola Superior de Tecnologia de Setúbal, Instituto Politécnico de Setúbal, 2914-508 Setúbal, Portugal
[2] Fábrica da Pólvora de Barcarena, Atlantica—Instituto Universitário, 2730-036 Barcarena, Portugal
[3] IST, Instituto Superior Técnico, Universidade de Lisboa, Av. Rovisco Pais, 1049-001 Lisboa, Portugal; madalena.barata.garcia@tecnico.ulisboa.pt (M.B.G.)
[4] IDMEC, Instituto Superior Técnico, Universidade de Lisboa, Av. Rovisco Pais, 1049-001 Lisboa, Portugal; virginia.infante@tecnico.ulisboa.pt (V.I.); pedro.amaral@tecnico.ulisboa.pt (P.M.A.)
* Correspondence: joao.ribeiro@estsetubal.ips.pt

Highlights

What are the main findings?

- Bending strength and failure modes were unaffected by aging.
- Aged specimens exhibit reduced flexural stiffness and lower shear rigidity relative to unaged samples.

What are the implications of the main findings?

- Durability in terms of strength is promising. The stability of bending strength after aging suggests that the composite retains its load-bearing capacity over time, making it suitable for long-term applications.
- Consistent failure mechanisms improve predictability. The unchanged failure modes between aged and unaged samples support reliable modeling and structural assessment across the composite's lifespan.

check for updates

Academic Editor: Martin J. D. Clift

Received: 9 October 2025
Revised: 2 December 2025
Accepted: 11 December 2025
Published: 18 December 2025

Citation: Marques, J.; Garcia, M.B.; Infante, V.; Amaral, P.M.; Correia, A. Aging Effects on Flexural Behavior of Glass Fiber-Reinforced Stone-Cork Composite Panels for External Facade Elements. *Fibers* **2025**, *13*, 167. https://doi.org/10.3390/fib13120167

Copyright: © 2025 by the authors. Licensee MDPI, Basel, Switzerland. This article is an open access article distributed under the terms and conditions of the Creative Commons Attribution (CC BY) license (https://creativecommons.org/licenses/by/4.0/).

Abstract

The building sector faces sustainability issues due to its substantial resource demand, prompting the exploration of alternative materials of natural origin. Given the diverse environmental conditions buildings experience, assessing the impact of these conditions on the mechanical characteristics of alternative materials becomes crucial. This study focuses on a composite comprising stone, agglomerate cork core and glass fiber-reinforced epoxy skins, designed for ventilated facades. The composite underwent an aging cycle commonly applied in the evaluation of construction building materials to evaluate its flexural behavior. To that end, bending tests on unaged and aged samples were carried out to investigate both the bending strength and stiffness. The composite panels were tested in two configurations: (i) stone facing up and (ii) stone facing down. The results indicated that higher bending strength was found in samples where the stone was facing up, regardless of the aging condition. In the stone facing up configuration, the predominant failure mode was stone crushing, whereas the samples in the stone facing down configuration evidenced a failure mechanism of fiber breakage. Despite the observed morphological differences between aged and unaged specimens, no significant difference was found regarding the bending strength and failure modes in both tested configurations. However, a flexural stiffness reduction of at least 21% was found for every aged specimen.

Keywords: GFRE; natural materials; sandwich composites; aging; mechanical characterization

1. Introduction

The building sector requires a great quantity of resources as highlighted by data found in the European Union: 42% of the total final energy consumption, 35% of greenhouse gas emissions, 50% of extracted materials and finally, 30% of water consumption and waste generation [1]. These alarming statistics have brought the sector into political agendas in order to improve the sustainability of the sector. Introducing alternative natural materials has emerged as a trend to enhance sector sustainability [1]. However, there is a crucial need to comprehensively understand the behavior of these alternatives under the typical environmental conditions which buildings experience over their lifespan. This evaluation is essential to ascertain the performance of these materials after prolonged exposure to such conditions. The aging phenomenon on composites has been studied by the scientific community. An example of this can be observed in the study conducted by N. Belayachi et al. [2] which evaluated the impact of accelerated aging on gypsum plaster–straw composite used for building thermal insulation. The results indicated that drying-wetting cycles promoted significant changes to the mechanical properties of the composite, while the freezing-thawing cycle led to less significant changes to the same properties. C. Kim and C. Hong [3] established a correlation between accelerated and natural aging tests on a graphite–epoxy composite. After 2000 h of accelerated aging, specimens presented a 17.5% reduction in stiffness compared to the unaged specimens. A similar analysis was performed only considering resin and revealed an 8% reduction in stiffness for the same time frame. As for natural aging, a five-year period was considered, and a 23% longitudinal flexural stiffness reduction was found, with matrix cracking and loss on aged specimens. This study also aligns with the investigation by L. Xu [4], emphasizing the role of matrix cracking on stiffness reduction in glass fiber-reinforced polymer (GRP) laminates. M. Najafi et al. [5] analyzed the effect of water on a symmetric sandwich composite composed of agglomerated cork and two glass fiber–epoxy skins. The stiffness reduction was more severe when the specimen was immersed in water without sealing (45.85 N/mm). However, the sealed scenario presented a considerable stiffness reduction compared to the dried scenario (63.14 and 103.81 N/mm, respectively). A similar trend was found by Kumar et al. [6]. In that work, foam was used as a core material instead and the specimens were aged with seawater. A stiffness reduction of 43% was found when compared to the undamaged scenario. In the same line, F. Avilés and M. Aguilar-Montero [7] found a 67% stiffness reduction on a symmetric sandwich composite composed of polyvinyl chloride (PVC) foam core and E-glass–polyester skins after 90 days' exposure to seawater. However, the elastic modulus of GFRP bars when exposed to seawater at 60 °C did not show significant variation. On the other hand, the impact of the aging cycle was more severe on the tensile strength [8]. These conclusions were reiterated in a comprehensive review performed by S. Li et al. [9] regarding the effect of aging in seawater environments on GFRP composites. G. Hota et al. [10] investigated the degradation mechanisms of glass fiber/vinyl ester-based composite materials through both accelerated and natural aging. Their findings revealed a notable reduction in interlaminar shear strength as exposure temperature and duration increased, particularly evident within alkaline environments. Building on the knowledge garnered from prior research on the natural aging of such composites, this study successfully established a correlation between accelerated and natural aging. Employing the Arrhenius model and the time–temperature superposition principle,

the results demonstrated that accelerated aging tests spanning 150 days equate to nearly 3 years of real-world exposure. Furthermore, extended accelerated aging surpassing this timeframe was shown to correlate with up to 27 years of natural degradation. K. Mak and A. Fam [11] evaluated the performance of flax-FRP (FFRP) and glass-FRP (GFRP) sandwich panels which were subjected to different ambient temperatures (−20 °C, 0 °C and 20 °C) for a minimum of 1 h. These panels were tested under a four-point bending configuration. The outcomes of this work showed that, in the case of GFRP sandwich panels, a reduction in bending strength was found as the ambient temperature increased. However, there was no considerable variation observed in the tensile modulus. On the other hand, for FFRP, no significant variation in strength was found, while the tensile modulus decreased as the temperature increased. M. Khotbehsara et al. [12] studied the aging of particulate-filled epoxy resin under hygrothermal conditions. In this work, the material was subjected to temperatures up to 60 °C and relative humidity of 98% for durations of 1000, 2000 and 3000 h. The findings revealed that hygrothermal conditions altered the failure behavior (from brittle to semi-ductile), and a reduction of less than 10% was found in tensile and compressive strength. A. Manalo et al. [13] demonstrated that the strength and stiffness of pultruded GFRP composite laminates significantly decreased when exposed to temperatures ranging from 100 °C and 150 °C due to the glass transition of the vinyl ester resin. J. Almeida et al. [14] evaluated the effects of conditioning carbon fiber–epoxy laminates at 80 °C and a relative humidity of 90% for 60 days. It was found that there was a reduction in shear strength and modulus of approximately 30% and 38%, respectively. This reduction was attributed to water absorption which caused plasticization of the matrix and induced stresses. H. Fergani et al. [15] assessed the durability of GFRP subjected to severe environments, including moist concrete, alkaline solution and tap water, across a temperature range of 20 °C to 60 °C. The outcomes highlighted the significant influence of higher temperatures in initiating and accelerating the development of critical degradation mechanisms. Furthermore, the long-term mechanical properties of the tested GFRP bars appeared to be primarily influenced by moisture diffusion through the resin-rich layer and debonding at the fiber/matrix interfaces. S. Swain et al. [16] compared the durability of GFRP composites exposed to outdoor weathering and an aging cycle carried out using laboratory apparatus (95% of relative humidity at 60 °C). Despite the laboratory conditions leading to a higher moisture intake, interlaminar shear stress decreased more significantly when samples were subjected to outdoor conditions. Regarding the use of GFRP sandwich panels in the construction sector, P. Mazzuca et al. [17] investigated the fire performance of glass fiber-reinforced polymer sandwich panels produced by vacuum infusion. Eleven four-point bending tests were conducted under sustained load and ISO 834 standard fire exposure [18] to assess the influence of different foam cores (PUR and PET), the presence of longitudinal GFRP webs and two passive fire protection systems. The results showed that panels with longitudinal webs achieved superior fire resistance due to enhanced shear performance, while the addition of calcium silicate (CS) boards (especially in suspended configurations) significantly increased fire endurance, extending collapse times up to 90 min.

In the present work, an asymmetric sandwich composite composed of stone, agglomerate cork and two GFRE layers is characterized and subjected to an accelerated aging cycle applied to construction materials. Four-point bending tests were performed in order to assess the effect of such an aging cycle on the bending strength, flexural stiffness and transverse shear rigidity of this composite.

2. Materials and Methods

2.1. Materials

The specimens consisted of a core of cork agglomerate (CA) sandwiched between two glass fiber-reinforced epoxy (GFRE) skins, along with a structural natural material (natural stone) [19], as illustrated in Figure 1.



Figure 1. Schematic of the asymmetric composite panel [20].

The stone layer utilized Creme de Fátima limestone (Table 1) [21], sourced from Filstone (Fátima, Portugal), while the CA, NL20 (Table 2) [22], was supplied by Amorim Cork Composites (Mozelos, Portugal) with an average thickness of 15 mm. To produce glass fiber skins, this composite material employed Epolit RS 7720 epoxy resin (Table 3) provided by QMC Tecnología Química (Valencia, Spain) [23], along with two different glass fibers. To ensure a balanced stiffness transition between the stone and agglomerated cork, a stiffer glass fiber, EBXS600 (Table 4) from Castro Composites (Porriño, Spain) [24], was used for the GFRE1 layer, while the GFRE2 layer employed UTE 280 T fiber (Table 5) [25], also from Castro Composites. This second layer was used to increase the overall ductility of the composite. The fibers within this composite play a crucial role in its mechanical properties. Without their reinforcing contribution, the stiffness gradient between the stone and cork layers would remain too abrupt, preventing compatible deformation and leading to detrimental relative movement between the layers. Such behavior would promote premature fracture of the stone layer, even at low deflection levels, ultimately compromising the structural integrity of the system. Additionally, they further enhance the ductility of the composite, ensuring that the composite can deform without inducing early cracking in the stone layer. The mass ratio between the resin and total (resin + fiber) was around 70%. The curing process consisted of 75 min under a hot-press with a defined temperature of 55 °C. A post-curing stage was subsequently carried out for 6 h at 60 °C. The average dimensions for the specimens were 50 mm width, 23 mm total thickness and a length of 300 mm.

Table 1. "Creme de Fátima" limestone properties [21].

Apparent Density	**2500 kg/m^3**
Open porosity	7.52%
Water absorption	2.67%
Compression resistance	145.09 MPa
Bending resistance	14.25 MPa
Wear resistance	22.42 mm

Table 2. NL20 agglomerate cork properties [22].

Density	**170–235 kg/m^3**
Compressive strength	0.5 MPa
Compressive modulus	6.0 MPa
Tensile strength	0.4 MPa
Shear strength	0.9 MPa
Shear modulus	5.9 MPa

Table 3. Epolit RS 7720 properties [23].

Property	**Part A**	**Part B**
Viscosity at 25 °C	400–500 mPas	100–150 mPas
Density	1100 kg/m^3	1020 kg/m^3
Mixture ratio	100 (by weight)	25 (by weight)
Gel time 20 °C, 100 g	35–65 min	
Gel temperature T_g	80 °C	

Table 4. EBXS600 fiber properties [24].

Properties (Fabric)	
Knitting	Tricot
Theoretical mass/area	612 g/m^2
Fiber direction	Biaxial fabric 0° 90°
Properties (Filament Yarn)	
Density	2.59–2.62 g/cm^3
Filament dimeter	12–15 µm
Tensile strength	1900–2400 MPa
Tensile modulus	69–76 GPa
Elongation at break	3.5–4%

Table 5. UTE 280 T fiber properties [25].

Mass/Area	**300 g/m^2**	
Weave	Twill	
Tensile strength	Warp	3629 MPa
	Weft	2815 MPa

2.2. Aging Cycle

The specimens were aged under a cycle which is referred to as cycle A throughout the document. This cycle was based on the ASTM C481 standard "Standard Test Method for Laboratory Aging of Sandwich Constructions" [26]. It is worth mentioning that this standard proposes two aging cycles, cycle B being the one defined as the reference for this work. The aging cycle can be briefly described by the following steps:

- Immerse the specimen horizontally in room-temperature water for 24 h;
- Keep at 50 °C and relative humidity of 90% for 2 h;

- Heat in dry air (relative humidity: 15%) at 83 °C for 3.5 h;
- Cool to 70 °C;
- Spray the specimen in order to increase the overall humidity of the chamber (90% relative humidity). Keep for 6 h at 70 °C;
- Heat in dry air (relative humidity: 15%) at 83 °C for 18 h.

These steps were performed 6 times using the Fitoclima 300 EP20 climatic chamber, commercialized by Aralab (Lisbon, Portugal). The aging cycle was programmed using the CLIMAPLUS V software (version 2) developed by Aralab. Some adjustments were made to the selected aging cycle, especially regarding the first step of the cycle. The immersion time was greatly increased in this scenario to ensure the full saturation of the specimens.

Two batches, designated F and FA, were produced. In batch F, the specimens were not subjected to aging. In batch FA, 15 specimens were selected. Initially, 5 specimens were used to calculate flexural stiffness (without aging). Subsequently, all 15 specimens were aged, and the same 5 specimens were again tested to determine the flexural stiffness (aged condition). The remaining 10 specimens were then used for destructive testing.

2.3. Destructive Bending Tests

The methodology chosen was based on the one found in the ASTM C393/C393M [27] standard. The four-point bending third-point loading test was selected where the load is applied in two points at the same distance from the supports, one third of the supporting span (S), employing the experimental setup depicted in Figure 2.

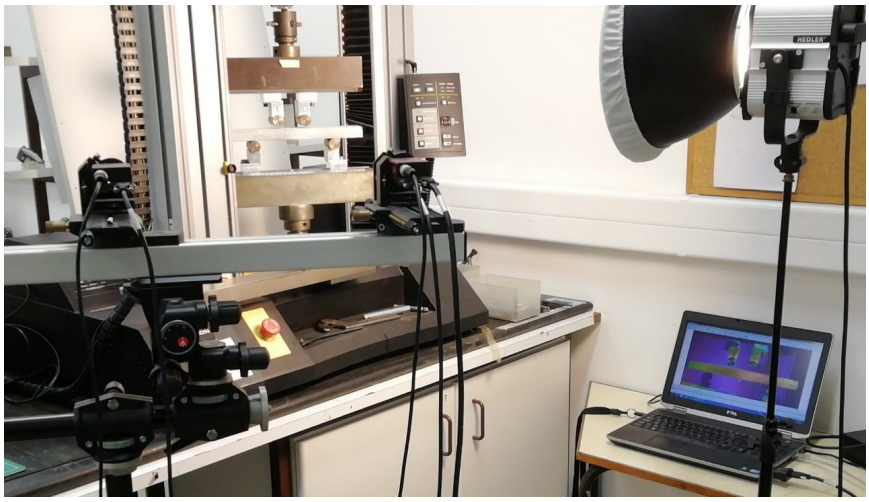


Figure 2. Experimental setup.

The bending tests were performed on a universal testing machine Instron 5566, using a 10 kN load cell. The tests were performed and controlled with a velocity of the top rollers of 3 mm/min, and a preload of about 10 N was applied before each test, as suggested by M. Garcia [28]. The testing machine was connected to Bluehill Universal software (version 4.44). This software recorded the load, displacement and time values throughout the different experimental tests with a frequency of 50 Hz. The specimens were tested in the stone facing up (stone in contact with the top rollers) and facing down configuration (stone in contact with the bottom rollers).

Flexural stiffness was determined using the methodology described in [29]. The mid-span deflection, Δ, can be given as a function of the applied load by Equation (1), according to Mancuso et al. [30] and based on the ASTM D7250/D7250M standard [31].

$$\Delta = \Delta_{bend} + \Delta_{shear} = \frac{P\left(2S^3 - 3SL^2 + L^3\right)}{96D} + \frac{P(S-L)}{4U} \quad (1)$$

where D is the flexural stiffness, while U corresponds to the transverse shear rigidity. Given the selected four-point bending test setup, ($L = S/3$), Equation (2) is obtained:

$$\left(\frac{\Delta}{SP}\right) = \frac{1.7}{96D}S^2 + \frac{1}{6U} \quad (2)$$

This equation can be transformed into a linear regression of the type $y = mx + b$ where m is the slope of the equation and b is the interception point with the y axis when plotting as a function of S^2. The flexural stiffness, D, can be determined from the slope, while the transverse shear rigidity, U, can be obtained using the interception point with the y axis. Both can be calculated using Equations (3) and (4), respectively.

$$D = \frac{1.7}{96m} \quad (3)$$

$$U = \frac{1}{6b} \quad (4)$$

This method consists of performing bending tests with the same loading configuration but increasing the supporting span length (S = 100 mm, S = 175 mm, S = 200 mm and S = 250 mm). To ensure that no deformation or damage occurred to the specimen, a maximum load of 25% of the value obtained from destructive bending tests, considering a supporting span of 250 mm, was applied. This method was carried out before and after exposing the specimens to the aging cycle. In this way, the effect of said cycle can be evaluated for the same specimen.

The mid-span deflection was computed as the difference between the deflection value in the middle of the specimen minus the deflection measured on top of the rollers. These values of deflection were taken from the final image of the VIC-2D software (version 7) analysis that measured the deflection throughout the test. Figure 3 shows a typical vertical displacement distribution obtained using DIC.

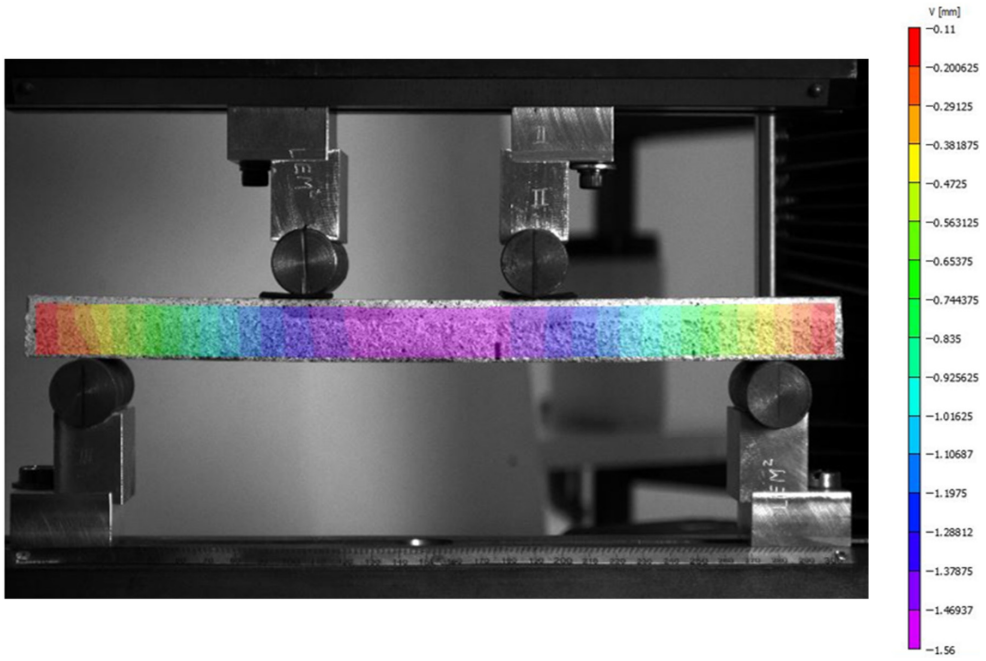


Figure 3. Typical vertical displacement field obtained from VIC 2D program.

Each specimen was tested 3 times for the different S values with a minimum resting time between tests of 30 min to ensure cork restitution [32]. Accordingly, the specimens are designated as FAi_j, where i ranges between 1 and 5 (five specimens) and j represents the

repetition number. It is important to note that in this case, the specimens were only tested in the stone facing up configuration.

3. Results

3.1. Morphologic Analysis Between Aged and Unaged Specimens

After the aging cycle and before testing the aged specimens, a morphologic comparison between the aged and unaged specimens was made to visualize the effects of the aging cycle upon the specimens (Figure 4).



Figure 4. Morphological comparison between aged (A) and unaged (U) specimens: (**a**) side view, (**b**) GFRE view.

Figure 4a shows that the agglomerated cork core, after the aging cycle, presented a darker shade compared to the unaged scenario. This comparison was made after drying the aged specimens, which indicated that this darker shade was not due to the presence of water. Moreover, Figure 4b demonstrates that, in the aged case, it is easier to discern the fiber's direction compared to the unaged case. This observation can lead to the hypothesis that the aging cycle may have caused degradation of the resin, partially exposing the fibers. However, a comprehensive mechanical characterization of both unaged and aged specimens is necessary to gain insight into the degradation of mechanical properties caused by the aging cycle.

3.2. Bending Strength

The stress vs. displacement curves for the stone facing up configuration and for both unaged and aged specimens can be found in Figures 5a and 5b, respectively. In parallel, the stress vs. displacement curves for the stone facing down configuration are presented in Figures 5a and 6a for unaged specimens and in Figures 5b and 6b for aged specimens.

Comparing Figures 5 and 6, it is evident that the composite has a higher bending strength in the stone facing up configuration since stone presents a higher resistance when in compression. Figure 5 demonstrates that once the maximum stress was reached, there was an abrupt stress reduction corresponding to the instant of failure for the specimens. In Figure 6, this trend was also observed; however, there were local maxima before reaching the maximum stress value. This behavior can be attributed to the breakage of certain fibers without leading to a catastrophic failure of the composite. Figures 7a and 7b display the comparison between the bending strength obtained for unaged and aged spec-

imens, along with the respective standard deviation for both stone facing up and down configurations, respectively.

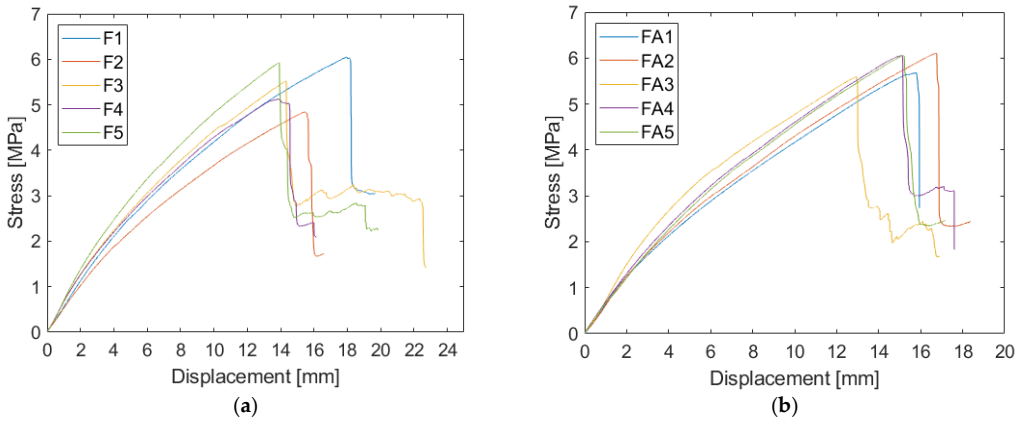


Figure 5. Stress vs. displacement curves for stone facing up configuration: (**a**) unaged and (**b**) aged specimens.

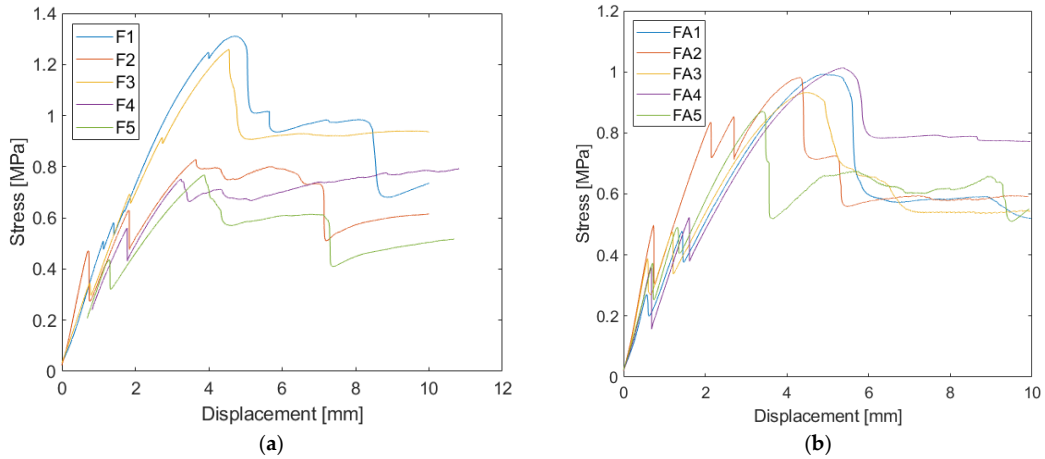


Figure 6. Stress vs. displacement curves for stone facing down configuration: (**a**) unaged and (**b**) aged.

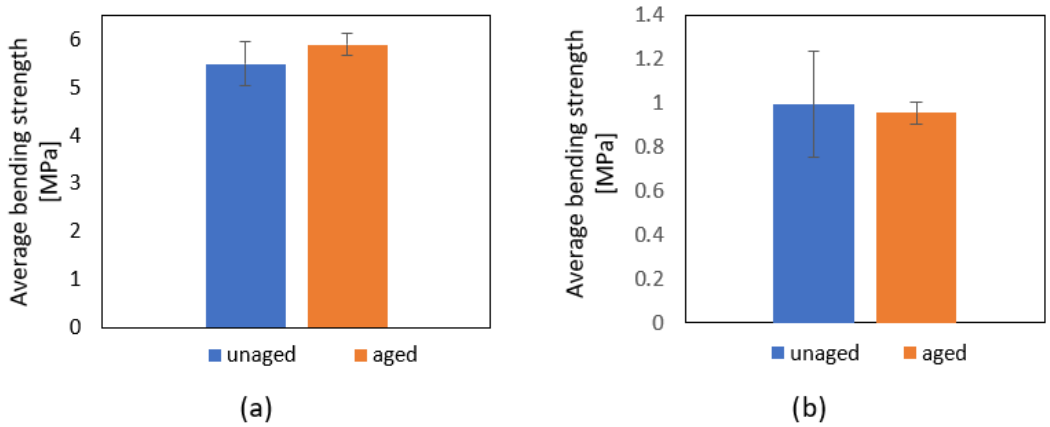


Figure 7. Average bending strength for unaged and aged specimens: (**a**) stone facing up configuration, (**b**) stone facing down configuration.

The similarity between the values for the unaged and aged specimens, in both cases, may indicate that the aging process did not have a significant effect on the materials concerning their bending strength, regardless of the testing configuration.

3.3. Failure Modes

As mentioned before, the composite material was tested in two different configurations: (i) stone facing up and (ii) stone facing down configuration. In both cases, a predominant failure mode was found: stone crushing (stone facing up configuration, Figure 8a) and fiber breakage (stone facing down configuration, Figure 8b).

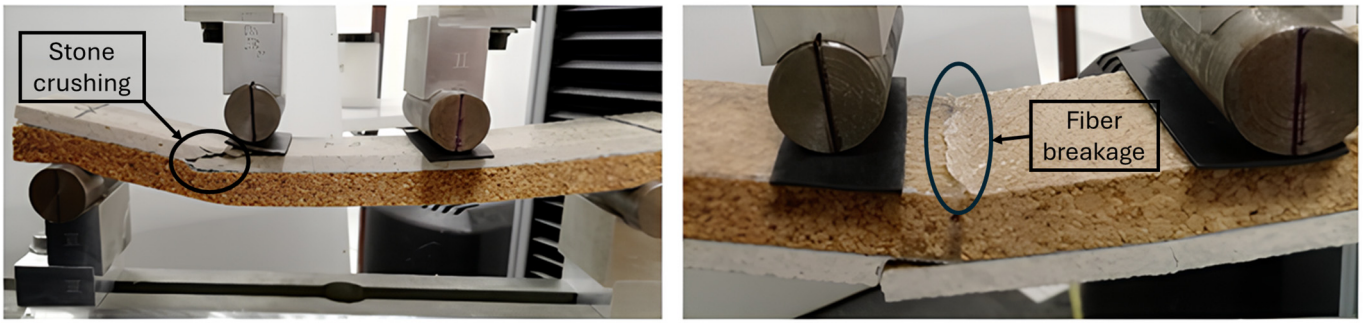


Figure 8. Failure modes observed in each testing configuration: (**a**) stone facing up and (**b**) stone facing down.

On the one hand, the stone facing up configuration was characterized by stone crushing beneath both loading rollers, yet not simultaneously. On the other hand, the stone facing down configuration revealed fiber breakage beneath both rollers, with the exception shown in Figure 8b, in which the GFRE failed in between the loading rollers.

3.4. Flexural Stiffness and Transverse Shear Rigidity

As mentioned before, the flexural stiffness can be obtained from Equation (3) which corresponds to the slope of Equation (2). Figures 9 and 10 represent the relation between $\Delta/(SP)$ and S^2 for the FA1 specimen for the unaged and aged conditions, respectively.

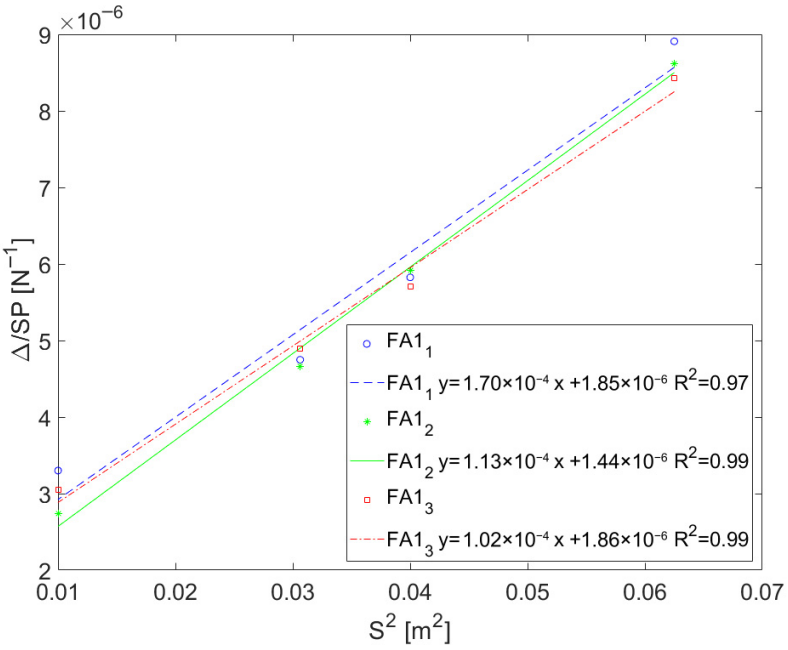


Figure 9. Relation between $\Delta/(SP)$ and S^2 for unaged FA1 specimen.

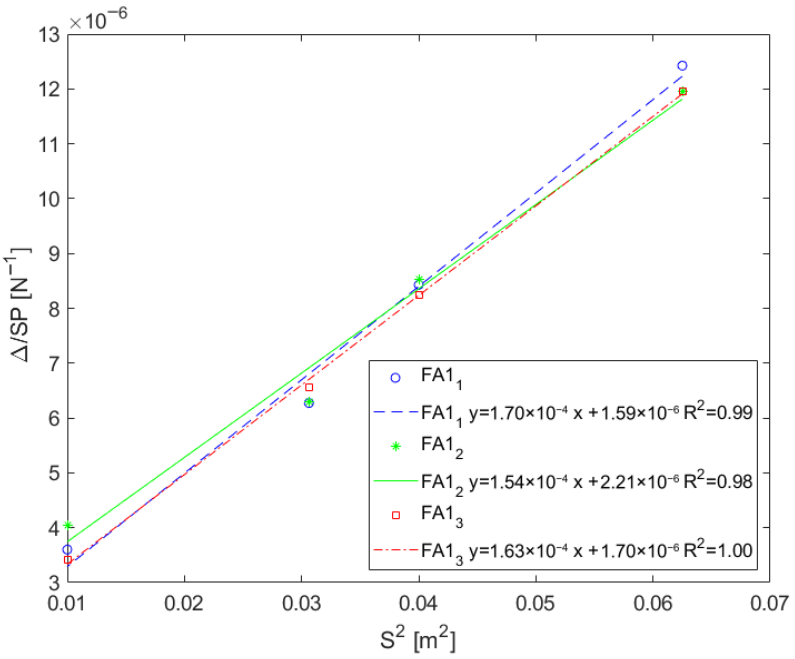


Figure 10. Relation between $\Delta/(SP)$ and S^2 for aged FA1 specimen.

From Figures 9 and 10, it is possible to observe that the different linear relations for both unaged and aged specimens presented determination coefficients higher than 0.97, which proves the linearity between $\Delta/(SP)$ and S^2. The three slopes within the same condition presented similar values, validating the setup used to acquire the data and carry out the experimental tests. Additionally, the three slopes obtained for unaged specimens were lower than slopes obtained for aged specimens. This indicates that, for the same span and applied force, the unaged specimen exhibited lower deflection. Using the obtained slope values and applying Equation (3), the different stiffness values can be obtained. Tables 6 and 7 present the stiffness values obtained for both unaged and aged specimens, respectively.

Table 6. Stiffness values for each test and respective average and standard deviation for batch FA before aging.

Batch	Specimen	D_1 [N.mm^2]	D_2 [N.mm^2]	D_3 [N.mm^2]	$\bar{D}$ [N.mm^2]	SD [N.mm^2]
FA	FA1	164.68	156.82	173.28	164.93	6.72
	FA2	148.30	129.01	137.15	138.15	7.91
	FA3	160.63	145.27	156.01	153.97	6.43
	FA4	188.64	194.51	206.69	196.61	7.52
	FA5	179.04	181.91	165.99	175.65	6.93

Table 7. Stiffness values for each test and respective average and standard deviation for batch FA after aging.

Batch	Specimen	D_1 [N.mm^2]	D_2 [N.mm^2]	D_3 [N.mm^2]	$\bar{D}$ [N.mm^2]	SD [N.mm^2]
FA	FA1	102.17	114.89	100.44	105.83	6.44
	FA2	94.13	109.23	113.84	105.73	8.42
	FA3	107.53	130.66	98.52	112.24	13.54
	FA4	142.74	132.52	191.07	155.44	25.54
	FA5	110.78	127.8	130.43	123.00	8.71

The data provided in Tables 6 and 7 reveals that the standard deviation found for stiffness exceeded 9 N.mm^2 only in specimens FA3 and FA4. When compared to the actual stiffness values, this suggests that both the method and setup (including the different equipment used) provided consistent values across the various repetitions.

As the stiffness parameter was obtained for the same batch (FA) before and after aging, it allowed for a direct comparison between both values to assess the influence of the aging cycle on this parameter. Figure 11 shows the average stiffness values and their respective standard deviations before and after the aging cycle for each specimen.

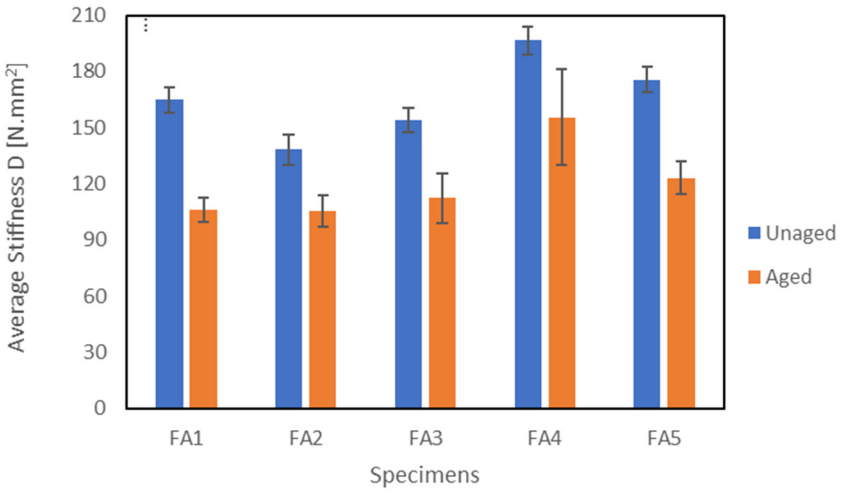


Figure 11. Average stiffness value and respective standard deviation before and after aging.

The results depicted in Figure 11 clearly indicate that the aging cycle led to a reduction in stiffness for every specimen. This reduction exceeded 21% in all cases. Among the aged specimens, FAS4 exhibited the highest variability in results (highest standard deviation), although the stiffness values consistently remained lower than those of the unaged specimens. Given that flexural stiffness in asymmetric sandwich composites is primarily governed by the stiffness of the face sheets, the shift in the neutral axis toward the stiffer stone layer becomes decisive in controlling the bending behavior [20]. Any degradation affecting the stone face or the neighboring interface therefore has a disproportionate impact on the overall flexural response. The analysis, conducted on the same set of specimens before and after aging, strongly suggests that the aging cycle contributed to a reduction in flexural stiffness. The transverse shear rigidity can also be obtained from Equation (2). However, this parameter was derived from the interception point with the y axis of the linearized curves found in Figures 9 and 10, in accordance with Equation (4). In Tables 8 and 9, the values of transverse shear rigidity can be found for the unaged and aged specimens, respectively.

Table 8. Shear rigidity values for each test and respective average and standard deviation for batch FA before aging.

Batch	Specimen	U_1 [kN]	U_2 [kN]	U_3 [kN]	$\bar{U}$ [kN]	SD [kN]
FA	FA1	90.09	115.74	89.61	98.48	12.21
	FA2	100.40	148.81	146.20	131.80	22.23
	FA3	73.10	101.01	90.09	98.48	11.48
	FA4	97.47	93.63	92.08	94.39	2.26
	FA5	68.31	62.89	73.75	68.32	12.21

Table 9. Shear rigidity values for each test and respective average and standard deviation for batch FA after aging.

Batch	Specimen	U_1 [kN]	U_2 [kN]	U_3 [kN]	$\bar{U}$ [kN]	SD [kN]
FA	FA1	104.82	75.41	98.04	92.76	12.57
	FA2	40.95	38.31	33.07	37.44	3.28
	FA3	52.41	43.98	54.82	50.40	4.65
	FA4	39.97	40.36	30.98	37.10	4.33
	FA5	40.06	41.05	34.01	38.38	3.11

From the analysis of both Tables 8 and 9, it is possible to observe that the shear rigidity values of the aged specimens presented lower standard deviations. However, the lowest standard deviation was found for specimen FA2 before aging. Overall, the standard deviation levels across all repetitions were significantly lower compared to the corresponding average values for each specimen, further confirming the consistency of the results obtained in the three repetitions. As performed for the flexural stiffness, the average transverse shear rigidity before and after aging was also compared, as presented in Figure 12.

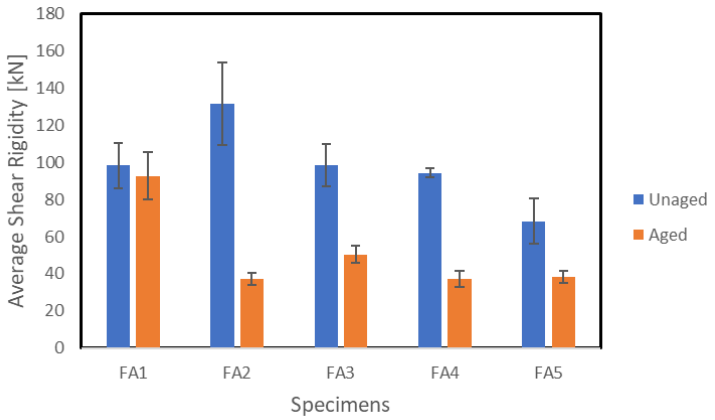


Figure 12. Average shear rigidity value and respective standard deviation before and after aging.

The analysis of Figure 12 shows a clear reduction in shear rigidity for the majority of the specimens after the aging cycle, which was also observed for the flexural stiffness parameter. However, in this case, this reduction was not found for all specimens, as the average shear rigidity for specimen FA1 remained nearly the same before and after aging, which may represent an outlier scenario. For the remaining cases, the reduction was always higher than 40%, which was notably higher than the reduction found for flexural stiffness. Since shear rigidity is governed by the core and interfacial capacity to transmit shear stresses between the asymmetric face sheets, the results indicate that aging primarily weakens this load-transfer mechanism, leading to an increased contribution of shear deformation to the overall structural response.

Overall, the results clearly show that the aging cycle affected both flexural stiffness and transverse shear rigidity, with aged specimens presenting lower values of both parameters. The decrease in flexural stiffness reflects changes in the stone face sheet, which largely governs the bending response in this asymmetric sandwich configuration. In contrast, the more pronounced reduction in transverse shear rigidity indicates that the cork core and the interfacial bonding were more vulnerable to aging. Nevertheless, the applied aging cycle did not induce sufficient degradation to trigger delamination or cork failure, as neither of these mechanisms were observed.

4. Conclusions and Further Works

This study contributes to the understanding of the mechanical behavior and durability of innovative stone–cork–GFRP sandwich composites for ventilated façade applications. The main original contributions of this work are outlined below, followed by the key conclusions drawn from the experimental results and the directions proposed for future research.

Original Contributions:

- Quantitative evaluation of pre- and post-aging flexural stiffness and transverse shear rigidity on the same specimens.
- Development of an asymmetric failure-mode map for stone–cork–GFRP façade panels.
- Assessment of stiffness reduction mechanisms under controlled aging cycles representative of façade surface exposure.

The behavior of an asymmetric sandwich composite, composed of stone, agglomerate cork and two GFRE layers, was evaluated under four-point bending in two configurations: with the stone facing up and with the stone facing down. The composite was tested both before and after an accelerated aging cycle in order to assess the cycle's influence on bending strength, failure modes, flexural stiffness, and transverse shear rigidity. From the results obtained, it can be concluded that

- The composite presented higher bending strength in the stone facing up configuration, due to stone presenting greater resistance under compression.
- For the stone facing up configuration, the predominant mode was stone crushing, while for the stone facing down configuration, the predominant failure mode was fiber breakage.
- Bending strength remained similar between unaged and aged specimens despite morphological differences.
- The failure modes were consistent across both aged and unaged specimens.
- Aged specimens presented lower flexural stiffness and lower shear rigidity compared to the unaged specimens.

The findings show that the aging cycle reduced both flexural stiffness and transverse shear rigidity; however, the bending strength and failure mechanisms remained stable. This indicates that the material's structural integrity is not compromised by the tested environmental exposure, and the stiffness reduction may even serve as a practical indicator for long-term condition monitoring of façade panels.

Overall, the stone–cork–GFRP composite maintained its mechanical performance despite the loss in stiffness, demonstrating resilience to aging effects. Its ability to endure environmental cycling without strength degradation underscores its suitability as a durable and sustainable solution for ventilated façade applications.

Future research will expand the present study by investigating additional aging conditions, such as freeze–thaw cycles, to evaluate the material's behavior under low-temperature and moisture fluctuations. Controlled ultraviolet (UV) exposure tests are also planned to assess the effects of photodegradation on the material's surface and mechanical properties. In addition, long-term outdoor exposure under real climatic conditions is planned to validate the laboratory findings and provide a more comprehensive understanding of the material's durability and performance throughout its service life. After that, it is planned to test façade plates under different aging cycles to corroborate the influence of said aging cycles but also the influence of said cycles on the connection between the façade plate and the supports.

Author Contributions: Conceptualization, J.M., M.B.G., V.I. and P.M.A.; Methodology, J.M. and M.B.G.; Software, J.M.; Validation, J.M. and M.B.G.; Formal analysis, J.M.; Investigation, J.M.; Resources, J.M.; Data curation, J.M.; Writing—original draft, J.M.; Writing—review & editing, A.C.; Visualization, J.M. and A.C.; Supervision, V.I. and P.M.A.; Project administration, V.I. and P.M.A.; Funding acquisition, P.M.A. All authors have read and agreed to the published version of the manuscript.

Funding: This research received no external funding.

Data Availability Statement: The data presented in this study are available on request from the corresponding author.

Acknowledgments: The authors gratefully acknowledge the following funding source: INOVSTONE4.0 (POCI-01-0247-FEDER-024535), co-financed by the European Union through the European Regional Development Fund (FEDER). This work was also supported by FCT through the PD/BD/140208/2018 scholarship.

Conflicts of Interest: The authors declare no conflicts of interest.

References

1. Kylili, A.; Fokaides, P.A. Policy trends for the sustainability assessment of construction materials: A review. *Sustain. Cities Soc.* **2017**, *35*, 280–288. [CrossRef]
2. Belayachi, N.; Hoxha, D.; Slaimia, M. Impact of accelerated climatic aging on the behavior of gypsum plaster-straw material for building thermal insulation. *Constr. Build. Mater.* **2016**, *125*, 912–918. [CrossRef]
3. Shin, K.B.; Kim, C.G.; Hong, C.S. Correlation of accelerated aging test to natural aging test on graphite—Epoxy composite materials. *J. Reinf. Plast. Compos.* **2003**, *22*, 849–861. [CrossRef]
4. Xu, L. Interaction Between Matrix Cracking and Edge Delamination in Composite Laminates. *Compos. Sci. Technol.* **1994**, *50*, 469–478. [CrossRef]
5. Najafi, M.; Darvizeh, A.; Ansari, R. Characterization of moisture effects on novel agglomerated cork core sandwich composites with fiber metal laminate facesheets. *J. Sandw. Struct. Mater.* **2020**, *22*, 1709–1742. [CrossRef]
6. Kumar, S.J.A.; Ahmed, K.S. Effects of ageing on mechanical properties of stiffened syntactic foam core sandwich composites for marine applications. *J. Cell. Plast.* **2016**, *52*, 503–532. [CrossRef]
7. Avilés, F.; Aguilar-Montero, M. Mechanical degradation of foam-cored sandwich materials exposed to high moisture. *Compos. Struct.* **2010**, *92*, 122–129. [CrossRef]
8. Morales, C.N.; Claure, G.; Emparanza, A.R.; Nanni, A. Durability of GFRP reinforcing bars in seawater concrete. *Constr. Build. Mater.* **2021**, *270*, 121492. [CrossRef]
9. Li, S.; Guo, S.; Yao, Y.; Jin, Z.; Shi, C.; Zhu, D. The effects of aging in seawater and SWSSC and strain rate on the tensile performance of GFRP/BFRP composites: A critical review. *Constr. Build. Mater.* **2021**, *282*, 122534. [CrossRef]
10. Hota, G.; Barker, W.; Manalo, A. Degradation mechanism of glass fiber/vinylester-based composite materials under accelerated and natural aging. *Constr. Build. Mater.* **2020**, *256*, 119462. [CrossRef]
11. Mak, K.; Fam, A. Performance of flax-FRP sandwich panels exposed to different ambient temperatures. *Constr. Build. Mater.* **2019**, *219*, 121–130. [CrossRef]
12. Khotbehsara, M.M.; Manalo, A.; Aravinthan, T.; Ferdous, W.; Nguyen, K.T.Q.; Hota, G. Ageing of particulate-filled epoxy resin under hygrothermal conditions. *Constr. Build. Mater.* **2020**, *249*, 118846. [CrossRef]
13. Manalo, A.; Maranan, G.; Sharma, S.; Karunasena, W.; Bai, Y. Temperature-sensitive mechanical properties of GFRP composites in longitudinal and transverse directions: A comparative study. *Compos. Struct.* **2017**, *173*, 255–267. [CrossRef]
14. Almeida, J.H.S.; Souza, S.D.B.; Botelho, E.C.; Amico, S.C. Carbon fiber-reinforced epoxy filament-wound composite laminates exposed to hygrothermal conditioning. *J. Mater. Sci.* **2016**, *51*, 4697–4708. [CrossRef]
15. Fergani, H.; Di Benedetti, M.; Oller, C.M.; Lynsdale, C.; Guadagnini, M. Durability and degradation mechanisms of GFRP reinforcement subjected to severe environments and sustained stress. *Constr. Build. Mater.* **2018**, *170*, 637–648. [CrossRef]
16. Swain, S.; Beura, S.; Thatoi, D.N.; Chakraverty, A.P.; Mohanty, U.K. Durability of GFRP composite exposed to outdoors weathering. *Compos. Commun.* **2019**, *13*, 22–29. [CrossRef]
17. Mazzuca, P.; Firmo, J.P.; Correia, J.R.; Rosa, I.C. Fire behaviour of vacuum-infused glass fibre reinforced polymer sandwich panels: The role of polyurethane and polyethylene terephthalate foam cores and panel architecture. *Eng. Struct.* **2025**, *345*, 121411. [CrossRef]
18. *ISO 834*; Fire Resistance Tests. Elements of Building Construction: Geneve, Switzerland, 2018.

19. Amaral, P.; Pinheiro, J. Multilayer Laminate Panel. W.O. Patent No. 2017/021505 A1, 9 February 2017.
20. Marques, J.; Garcia, M.; Infante, V.; Amaral, P. Damage assessment on an asymmetric sandwich composite made of natural materials using strain gauges. *Eng. Fail. Anal.* **2024**, *160*, 108167. [CrossRef]
21. Filstone. Filstone Grey M Informação Técnica. Available online: https://filstone.com/blocos-de-calcario/filstone-grey-m/ (accessed on 15 September 2025).
22. Amorim Cork Composites. *NL20 Material Data Sheet*; Amorim Cork Composites: Mozelos, Portugal, 2013.
23. QMC Technical Datasheet Epolit RS 7720. Available online: https://iberdin.com/produto/resina-epoxi-epolit-rs-7700/ (accessed on 20 September 2025).
24. Castro Composites. *EBXS600 Technical Data Sheet*; Castro Composites: O Porriño, Spain, 2015.
25. Castro Composites. *UTE 280 T Technical Data Sheet*; Castro Composites: O Porriño, Spain, 2014.
26. *ASTM C481*; Standard Test Method for Laboratory Aging of Sandwich Constructions. ASTM International: West Conshohocken, PA, USA, 2016.
27. *ASTM C393/C393M-11*; Standard Test Method for Core Shear Properties of Sandwich Constructions by Beam Flexure. American Society for Testing and Materials: West Conshohocken, PA, USA, 2011.
28. Garcia, M. Characterisation of Adhesive Systems Used to Produce Multi-Layered Composites Made of Natural Materials. Master's Thesis, Instituto Técnico Lisboa, Universidade de Lisboa, Lisboa, Portugal, 2017.
29. Ribeiro, J.P.S. *Avaliação do Comportamento Mecânico de Estruturas Compósitas Tipo Sanduíche de Baixo Peso Específico Utilizando Materiais Naturais*; Instituto Superior Técnico: Lisboa, Portugal, 2016.
30. Mancuso, A.; Pitarresi, G.; Tumino, D. Mechanical Behaviour of a Green Sandwich Made of Flax Reinforced Polymer Facings and Cork Core. *Procedia Eng.* **2015**, *109*, 144–153. [CrossRef]
31. *ASTM D7250/D7250M*; Standard Practice for Determining Sandwich Beam Flexural and Shear Stiffness. American Society for Testing and Materials: West Conshohocken, PA, USA, 2011.
32. Ramos, M. *Produção e Caracterização de Materiais Compósitos à Base de Aglomerado de Cortiça*; Instituto Superior Técnico: Lisboa, Portugal, 2018.

Disclaimer/Publisher's Note: The statements, opinions and data contained in all publications are solely those of the individual author(s) and contributor(s) and not of MDPI and/or the editor(s). MDPI and/or the editor(s) disclaim responsibility for any injury to people or property resulting from any ideas, methods, instructions or products referred to in the content.